Center for Turbulence Research
Proceedings of the Summer Program 2010

Multi-scale modeling of compressible multi-fluid flows with conservative interface method

By X. Y. Hu†, N. A. Adams†, M. Herrmann‡ AND G. Iaccarino

One important issue associated with the complexity of dynamically evolving material interface is the scale-dependent dynamics which implies very different physical phenomena depending on the resolvability of the material interface. In this work we present a concept of multi-scale modeling where the interface interaction is modeled as being in mechanical non-equilibrium or in equilibrium, depending on a scale measure representing the resolvability of the interface. The work is based on our previously developed conservative method for compressible multi-fluid flows with sharp and resolved interfaces. To extend this method for multi-scale modeling, two important issues are addressed: (i) a scale-separation algorithm identifying interface resolvability as resolved and non-resolved regions; (ii) a non-resolved-interface model and its efficient coupling to the resolved-interface model.

1. Introduction

Compressible multi-fluid flows are relevant to many industrial applications. One important issue associated with the complexity of a dynamically evolving material interface is the scale-dependent dynamics which implies very different physical phenomena acting at the different resolution levels of the material interface. While a pressure disturbance propagates across a well-resolved interface with pure-material sound speed, it propagates across an unresolved interface with a mixture (M-mixture) sound speed which can be orders of magnitude smaller. Furthermore, the disturbance propagates across a diffusive interface with again another mixture (T-mixture) sound speed, whose magnitude lies between the two pure-material sound speeds. The underlying mechanism is that a disturbance propagates with a frozen, M-mixture or T-mixture, sound speed, that depends on whether there is local mechanical non-equilibrium (microscopic view with resolved interface), mechanical equilibrium (mesoscopic view with unresolved interface) or thermodynamic equilibrium (macroscopic view with miscible interface) between the two fluids. With a given spatial-temporal resolution limit these non-equilibrium and equilibrium phenomena usually coexist within a single flow and are characteristic for the different stages of interface interactions. For flow problems with the interaction of compressible multiple fluids, at early stages the interface is well resolved and the dominant interface interaction is characterized by a mechanical non-equilibrium. At intermediate stages, since small unresolved interface structures have been produced continuously, the dynamics is strongly affected by both mechanical non-equilibrium and equilibrium interface interactions. At later stages, the dominant interface interaction is characterized by thermodynamic equilibrium due to strong molecular diffusion effects. It is well established that the overall mixing efficiency is mainly determined by the early and intermediate stages.

† Lehrstuhl für Aerodynamik, Technische Universität München, 85748 Garching, Germany
‡ School for Engineering of Matter, Transport and Energy, Arizona State University

Non-equilibrium and equilibrium interface interactions are modeled very differently: the mechanical non-equilibrium is modeled with a resolved-interface model where a double-valued pressure at the interface is permitted; the mechanical equilibrium is modeled with an unresolved-interface model where the equilibrium pressure is applied; the thermodynamic equilibrium is modeled with a miscible-mixture model where both equilibrium pressure and temperature are applied. In order to simulate flows with coexisting non-equilibrium and equilibrium, these models, though operating at different characteristic scales, need to be combined.

In this work, we propose to explore a concept of multi-scale modeling where the interface interaction is modeled as mechanical non-equilibrium or equilibrium depending on a scale measure for resolvability of the interface. The work is based on our previously developed conservative method for compressible multi-fluid flows with sharp and resolved interfaces (Hu *et al.* 2006, Hu *et al.* 2008, Hu *et al.* 2009). In this finite-volume method the interface is presented by a level-set function and the interface interaction is modeled by solving a two-material Riemann problem. To extend this method for multi-scale modeling, two important issues are addressed: (i) the development of a scale-separation algorithm for identifying the resolved and unresolved interface; (ii) the implementation of a non-resolved-interface model and its coupling to the resolved-interface model with simple and efficient approaches.

2. Method

Assuming the fluid to be inviscid and compressible, the governing flow equations can be written as a system of conservation laws

$$\frac{\partial \mathbf{U}}{\partial t} + \nabla \cdot \mathbf{F}(\mathbf{U}) = 0 \quad \text{on } \Omega. \tag{2.1}$$

Here, $\mathbf{U} = (\rho, \rho\mathbf{v}, E)^T$ is the density of the conserved quantities of mass, momentum and total energy with relation $E = \rho e + \rho\mathbf{v}^2/2$, where e is internal energy per unit mass. $\mathbf{F}(\mathbf{U})$ represents the corresponding flux functions. When a material interface $\Phi(t)$ separates the domain Ω into two parts, the states of fluid 1 and fluid 2 are described by different equations of state (EOS). Here, we assume a general EOS with form

$$p = \Gamma(\rho)\rho e + f(\rho), \tag{2.2}$$

where p is pressure, $\Gamma(\rho)$ is Grüneisen coefficient. $\Gamma(\rho)$ and $f(\rho)$ are functions of density. Eq. (2.2) generalizes an adequate approximation to a wide variety of materials of interest. This includes material such as ideal gas, stiff gas, explosives and condense matters under high pressure.

2.1. *Conservative sharp-interface method*

The conservative sharp-interface method (Hu *et al.* 2006, 2009) is developed for compressible multi-fluid flow. It uses a standard finite volume approach modified by considering computational cells being cut by interface. A typical discretization with explicit first-order forward time difference as basic building block for the higher-order Runge-Kutta method, of the Eq. (2.1) for a considered fluid, say fluid 1, on a uniform two-dimensional

gird of size Δ can be written as

$$\begin{aligned}\alpha_{i,j}^{n+1}\mathbf{U}_{i,j}^{n+1} = \frac{\lambda}{\Delta}\alpha_{i,j}^{n}\mathbf{U}_{i,j}^{n} + \lambda\hat{\mathbf{X}}(\Delta\Gamma_{i,j}) \\ + \lambda\left[A_{i-1/2,j}\hat{\mathbf{F}}_{i-1/2,j} - A_{i+1/2,j}\hat{\mathbf{F}}_{i+1/2,j}\right] \\ + \lambda\left[A_{i,j-1/2}\hat{\mathbf{F}}_{i,j-1/2} - A_{i,j+1/2}\hat{\mathbf{F}}_{i,j+1/2}\right], \end{aligned} \tag{2.3}$$

where $\lambda = \Delta t/\Delta$, Δt is the time step size. $\alpha_{i,j}\mathbf{U}_{i,j}$, where $\alpha_{i,j}$ is volume fraction, and $\mathbf{U}_{i,j}$ are the conservative quantities in the cut cell and the cell-averaged density of conservative quantities, respectively. $A_{i+1/2,j}$, $A_{i,j+1/2}$, $A_{i-1/2,j}$ and $A_{i,j-1/2}$ are cell-face apertures. $\hat{\mathbf{F}}$ is the cell-face flux, which is obtained by high-order shock-capturing schemes, *e.g.*, WENO schemes (Jiang & Shu 1996; Hu *et al.* 2010), and $\hat{\mathbf{X}}\left[\Delta\Phi_{i,j}\right]$, where $\Delta\Phi_{i,j}$ is the interface segment within the cut cell, is the momentum and energy flux across the interface segment determined by the interface interaction. For a small cut cell or an empty cell a stable fluid state may not be obtained based on the time step calculated according to the full grid size CFL condition. Therefore, the fluid in those cells is mixed with that of their neighboring cells with large volume fractions. The exchanges of the conservative quantities due to mixing are calculated according to the averaged values. The conservative quantities are updated by

$$\alpha_{i,j}^{n+1}\mathbf{U}_{i,j}^{n+1} \leftarrow \alpha_{i,j}^{n+1}\mathbf{U}_{i,j}^{n+1} + \sum_{k}\mathbf{M}, \tag{2.4}$$

where the second term on the right hand side represents the sum of all mixing operations. The volume fraction, interface segment and cell-aperture are reconstructed from the associated signed distance function $\phi(x, y, t)$, i.e., the level set function, which gives the zero level set for the location of the interface (Osher & Sethain 1988). The advection of the interface is achieved by the equation

$$\phi_t + \mathbf{v}\cdot\nabla\phi = 0, \tag{2.5}$$

where $\mathbf{v}$ is the advection velocity of the fluids.

Note that, as indicated by Eq. (2.3), the conservative sharp-interface method is only suitable for problems with resolved interfaces for which there are well-defined geometries, such as volume fraction, cell-face aperture and normal direction, in every computational cell. For unresolved interface, which is usually featured by a non-single cut on the computational cell-face, since there are no well-defined geometries, the sharp-interface method can not be applied accurately.

2.2. *Multi-scale modeling*

2.2.1. *Two-scale grid system*

In the two-scale grid system, the equation of fluid dynamics, i.e., Eq. (2.1), is discretized on the coarse grid of size Δ and the advection equation of interface, i.e., Eq. (2.5), is discretized on the refined grid (Hermann 2005). As shown in Figure 1, an odd refinement ratio of $r = 3$ or 5 is used, with $\Delta = r\Delta_r$, where Δ_r is the grid size of the refined grid, and the two grids are such that the center of a computational cell on the coarse grid is also a grid point of the refined grid. Hence, the grid-point index on the refined grid is $(ri + k, rj + l)$, where $k, l = 1, ..., r$ for each i or j. In order to increase computational efficiency a narrow band is defined near the interface. As shown in Figure 1 the narrow band includes three interface layers of computational cells on the coarse grid. The first

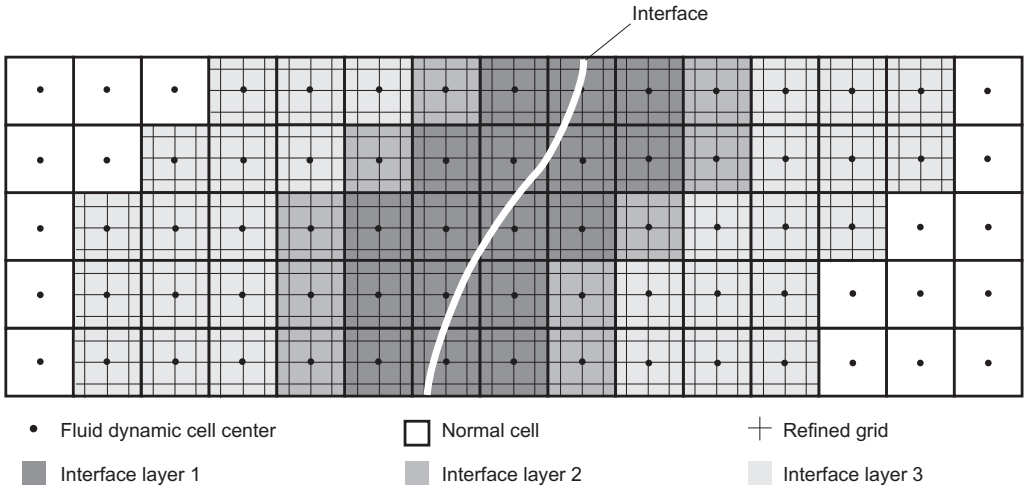

FIGURE 1. Schematic of the two-scale grid system with a refinement ratio of 3.

layer includes all cells where the refined grid is cut by the interface and their nearest neighbors. The second layer includes the nearest neighbor cells of the first layer and the third layer includes the first three nearest neighbor cells of the second layer.

2.2.2. *Reconstruction*

For a cell on the coarse grid the volume fraction and cell-face apertures are reconstructed by

$$\alpha_{i,j} = \frac{1}{r^2}\sum_{k,l=1}^{r}\left[n_x^2 H\left(\frac{\phi}{|\phi_x|},\Delta_r\right) + n_y^2 H\left(\frac{\phi}{|\phi_y|},\Delta_r\right)\right]_{ri+k,rj+l}, \tag{2.6}$$

$$A_{i+1/2,j} = \frac{1}{2r}\sum_{l=1}^{r}\left[H\left(\frac{\phi}{|\phi_y|},\Delta_r\right)_{ri+r,rj+l} + H\left(\frac{\phi}{|\phi_y|},\Delta_r\right)_{ri+r+1,rj+l}\right], \tag{2.7}$$

where $\mathbf{n} = (n_x, n_y) = (\phi_x, \phi_y)/\sqrt{\phi_x^2 + \phi_y^2}$ is the normal direction evaluated on a refined grid, and $H(z, \Delta_r)$ is a Heaviside function smoothed with scale Δ_r. Note that the cells with a volume fraction less than 0.5 are tagged as small cut cells, and the conservative quantities in them are mixed with their neighboring cells by a mixing procedure, as shown in Section 2.1.

2.2.3. *Scale separation*

The resolvability of the coarse grid with respect to the interface is identified based on a two-scale volume fraction measure. To obtain the volume fraction measured on the coarse grid, the level set on the refined grid within a coarse cell is first predicted from the values at the cell centers (each cell center coincides with a refined-grid point due to the set up of the grids, see Section 2.2.1.) by standard linear interpolation, and is used to predict the coarse-grid predicted volume fraction $\overline{\alpha_{i,j}}$ by Eq. (2.6). This volume fraction is then compared with the original value $\alpha_{i,j}$ calculated directly from the refined grid. If the difference is larger than a threshold value

$$|\alpha_{i,j} - \overline{\alpha}_{i,j}| > \epsilon, \tag{2.8}$$

the interface within this coarse cell is identified as unresolvable. As threshold we choose $\epsilon = 0.1$. Note that this scale measurement is very similar to that of Harten (1996) for calculating the scale coefficient.

2.2.4. *Interface advection*

The level set advection equation, i.e., Eq. (2.5), is solved by a semi-Lagrangian method (Strain 1999) on the first and second interface layers. Given the level set function for all grid points within the narrow band, the coordinate of the departure point $\mathbf{X}'_{ri+k,rj+l}$ for a grid point at coordinate $\mathbf{X}_{ri+k,rj+l}$ within the first and second interface layers is calculated by $\mathbf{X}'_{ri+k,rj+l} = \mathbf{X}_{ri+k,rj+l} - \mathbf{v}_{ri+k,rj+l}\Delta t$. The level set $\phi^{n+1}_{ri+k,rj+l}$ at the new time step is set with the value $\phi(\mathbf{X}'_{ri+k,rj+l})$, which is interpolated from the grid points around $\mathbf{X}'_{ri+k,rj+l}$. Here we use cubic Lagrangian interpolation for grid points within the first interface layer, and linear Lagrangian interpolation for grid points within the second interface layer to increase efficiency and numerical stability. The velocity $\mathbf{v}_{ri+k,rj+l}$ on the refined grid is approximated from the coarse grid with an B-spline filter, which prevents the creation of interface scales smaller than can be resolved by the refined grid (Pitsch 2005).

Note that since the semi-Lagrangian method is unconditionally stable for time integration, the time step Δt used for level-set advection is the same one as in Eq. (2.3). Also note that in order to maintain the level set function as singed distance to interface, reinitialization is implemented within all three interface layers except for the nearest-neighbor grid points of the interface to avoid erroneous interface shifting (Hu & Khoo 2004).

2.2.5. *Interaction at resolved interface*

For resolved interfaces on the coarse grid the sharp-interface method (Hu *et al.* 2006) can be applied directly. First, the interface velocity $\mathbf{v}_I$ and pressure p_I are obtained by solving a one-dimensional, two-material Riemann problem in the normal direction of interface (Hu & Khoo 2004, Hu *et al.* 2009). For the Riemann problem the state of the fluid which occupies the larger part of the volume fraction is updated from cell-averaged conservative quantities. The state of the other fluid is extended from the cells where this fluid has the larger part of the volume fraction (Fedkiw *et al.* 1999). With the interface velocity and interface pressure, the flux across the interface segment is calculated by

$$\hat{\mathbf{X}}^{\mathbf{P}}(\Delta\Gamma_{i,j}) = p_I \Delta\Gamma_{i,j}\mathbf{N}_I \quad \text{and} \quad \hat{X}^E(\Delta\Gamma_{i,j}) = p_I \Delta\Gamma_{i,j}\mathbf{N}_I \cdot \mathbf{v}_I, \tag{2.9}$$

where $\hat{\mathbf{X}}^{\mathbf{P}}$ stands for the momentum flux and $\hat{X}^E$ stands for the energy flux, and the approximated interface normal direction is $\mathbf{N}_I = (A_{i+1/2,j} - A_{i-1/2,j}, A_{i,j+1/2} - A_{i,j-1/2})/\Delta\Gamma_{i,j}$, where $\Delta\Gamma_{i,j} = \sqrt{(A_{i+1/2,j} - A_{i-1/2,j})^2 + (A_{i,j+1/2} - A_{i,j-1/2})^2}$.

2.2.6. *Interaction at an unresolved interface*

For an unresolved interface the one-dimensional Riemann problem is difficult to define because there is no well-defined interface normal direction. The interface interaction is solved based on a mechanical equilibrium model which assumes that the same cell-averaged velocity and pressure can be applied to both fluids within the cell, other than their respective interface values as for the resolved interface (Greenough *et al.* 1995). Assume the conservative quantities of two fluids in the cell are $\alpha_{i,j}\mathbf{U}^{(1)}_{i,j} = \left(\alpha U^{(1)}_1, \alpha \mathbf{U}^{(1)}_2, \alpha U^{(1)}_3\right)^T$ and $\beta_{ij}\mathbf{U}^{(2)}_{i,j} = \left(\beta U^{(2)}_1, \beta \mathbf{U}^{(2)}_2, \beta U^{(2)}_3\right)^T$, $\beta_{ij} = 1 - \alpha_{i,j}$, the cell-averaged density ρ_{ij}, ve-

locity $\mathbf{v}_{i,j}$ and internal energy $(\rho e)_{ij}$ can be obtained by

$$\rho_{ij} = \alpha U_1^{(1)} + \beta U_1^{(2)}, \tag{2.10}$$

$$\mathbf{v}_{i,j} = \frac{1}{\rho_{ij}} \left[\alpha \mathbf{U}_2^{(1)} + \beta \mathbf{U}_2^{(2)} \right], \tag{2.11}$$

$$(\rho e)_{ij} = \alpha U_3^{(1)} + \beta U_3^{(2)} - \frac{1}{2} \rho_{ij} \mathbf{v}_{i,j}^2. \tag{2.12}$$

The cell average pressure p_{ij} is obtained by a mixed EOS

$$p_{ij} = \frac{1}{\beta_{ij} \Gamma_{i,j}^{(1)} + \alpha_{i,j} \Gamma_{i,j}^{(2)}} \left[\Gamma_{i,j}^{(1)} \Gamma_{i,j}^{(2)} (\rho e)_{i,j} + \alpha_{ij} \Gamma_{i,j}^{(2)} f_{i,j}^{(1)} + \beta_{ij} \Gamma_{i,j}^{(1)} f_{i,j}^{(2)} \right]. \tag{2.13}$$

Note that in order to obtain $\Gamma_{i,j}^{(1)}$, $\Gamma_{i,j}^{(2)}$, $f_{i,j}^{(1)}$ and $f_{i,j}^{(2)}$, the densities $\rho_{i,j}^{(1)}$ and $\rho_{i,j}^{(2)}$ are required. Similar to the case of the resolved interface, for the fluid which occupies the larger part of the volume fraction the density is updated from the cell-averaged conservative quantities. For the other fluid it is extended from cells where this fluid has the larger part of the volume fractions. After interaction, except for the mass of the two fluids, conservative quantities change. With the condition of single-valued equilibrium cell-averaged velocity and pressure the conservative quantities after interaction can be calculated by

$$\alpha \mathbf{U}_2^{(1,*)} = \alpha U_1^{(1)} \mathbf{v}_{i,j}, \tag{2.14}$$

$$\beta \mathbf{U}_2^{(2,*)} = \beta U_1^{(2)} \mathbf{v}_{i,j}, \tag{2.15}$$

$$\alpha U_3^{(1,*)} = \alpha_{i,j} (\rho e)_{i,j}^{(1,*)} + \frac{1}{2} \alpha U_1^{(1)} \mathbf{v}_{i,j}^2, \tag{2.16}$$

$$\beta U_3^{(2,*)} = \beta_{i,j} (\rho e)_{i,j}^{(2,*)} + \frac{1}{2} \beta U_1^{(2)} \mathbf{v}_{i,j}^2, \tag{2.17}$$

where the internal energies $(\rho e)_{i,j}^{(1,*)}$ and $(\rho e)_{i,j}^{(2,*)}$ are obtained from the EOS of the two fluids, respectively. Hence, the momentum and energy flux across the interface can be calculated by

$$\hat{\mathbf{X}}^{\mathbf{P}}(\Delta\Gamma_{i,j}) = \frac{1}{2\Delta t} \left[\beta \mathbf{U}_2^{(2)} - \alpha \mathbf{U}_2^{(1)} + \alpha \mathbf{U}_2^{(1,*)} - \beta \mathbf{U}_2^{(2,*)} \right], \tag{2.18}$$

$$\hat{X}^E(\Delta\Gamma_{i,j}) = \frac{1}{2\Delta t} \left[\beta U_3^{(2)} - \alpha U_3^{(1)} + \alpha U_3^{(1,*)} - \beta U_3^{(2,*)} \right]. \tag{2.19}$$

Note that Eqs. (2.18) and (2.19) are unconditionally stable due to the locally implicit approach in Eqs. (2.14) to (2.17) for the interface flux of momentum and energy.

3. Numerical Examples

Two numerical examples are considered to validate the proposed multi-scale method. The first example is a pure interface transportation case by which the two-scale grid system and the scale-separation algorithm are validated. In order to study the influence of multi-scale modeling on compressible multi-fluid flow, a shock-bubble interaction is also considered.

3.1. *Interface transportation*

We consider a case in which the interface deforms in the single-vortex flow as introduced by Bell *et al.* (1989).

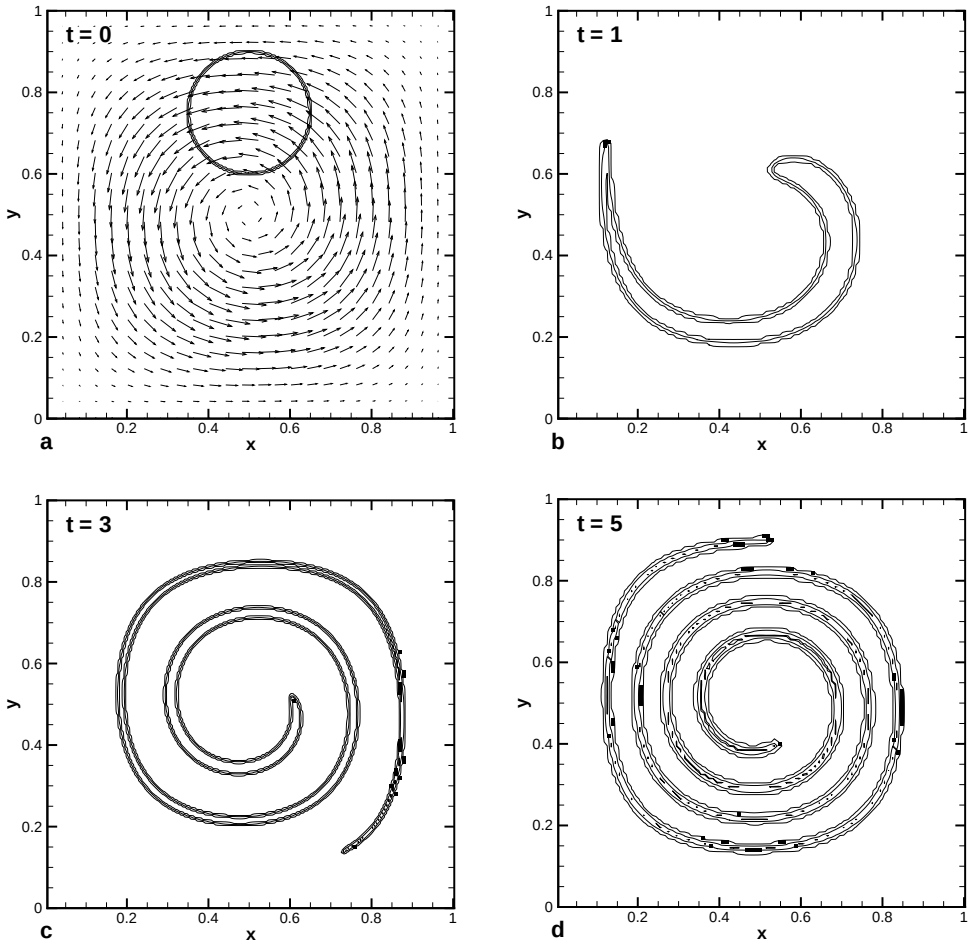

FIGURE 2. Results of interface deformation in the single vortex flow using a two-scale grid system ($\Delta = 0.01$, $r = 3$, volume fraction contours of $\alpha = 0.05$,0.5 and 0.95 obtained from level sets on the coarse grid): (a) initial interface location and velocity field, (b), (c) and (d) cells with unresolved interface (black squares) at time $t = 1$, 3, 5.

The initial interface, a circle placed at (0.5, 0.75) with radius 0.15, is shown in Figure 2a together with the velocity field:

$$u = -2\sin^2(\pi x)\sin(\pi y)\cos(\pi y), \tag{3.1}$$

$$v = 2\sin^2(\pi y)\sin(\pi x)\cos(\pi x). \tag{3.2}$$

The velocity field stretches the circle into a long filamentary structure which wraps itself around the center of the domain. As shown in Figure 2 b, c and d, the current semi-Lagrangian method obtains much more accurate results than the traditional level set method, but, since a low refinement ratio $r = 3$ is used, produces slightly larger errors

than the particle level set method (Hieber & Koumoutsakos 2005). Note that the current scale-separation algorithm works quite well. As shown in Figure 2 b, c and d, at the early stages most of the interface is well resolved except for the cusp (see Figure 2b). After the interface has deformed further more and more regions become non-resolved (see Figure 2c and d). Also note that the non-resolved regions usually are near to the cusp and the narrow neck of interface filament structures.

3.2. *Shock-bubble interaction*

In this problem, we compute a Mach 6 air shock wave interacting with a cylindrical helium bubble. Numerical computations for the same problem can be found in Hu *et al.* (2006). For this case the initial conditions in a computational domain $[0,1]\times[0,0.5]$ are

$$\rho = 1, u = -3, v = 0, p = 1, \gamma = 1.4 \qquad \text{preshocked air} \tag{3.3}$$

$$\rho = 5.268, u = 2.752, v = 0, p = 41.83, \gamma = 1.4) \qquad \text{postshocked air} \tag{3.4}$$

$$\rho = 0.138, u = 0, v = 0, p = 1, \gamma = 1.667) \qquad \text{helium bubble} \tag{3.5}$$

$$\phi = -0.15 + \sqrt{(x-0.25)^2 + y^2} \qquad \text{levelset,} \tag{3.6}$$

where $\phi \leq 0$ represents the helium and $\phi > 0$ represents the air, depicting a helium bubble of radius 0.15 at (0,0.25) which is to be impacted by a shock wave initiated at $x = 0.05$. The computation has been carried out with two resolutions of $\Delta = 5\times10^{-3}$ and 2×10^{-3} with the same refinement ratio $r = 3$ for the two-scale grid system. The upper and lower boundaries are imposed with reflecting-wall boundary conditions and the left and the right boundaries imposed with an outflow boundary condition with constant extrapolation. For these cases, one-phase calculations are carried out with an adaptive central-upwind 6th-order WENO scheme (Hu *et al.* 2010), which gives very small numerical dissipation, and a 3rd-order TVD Runge-Kutta scheme (Shu & Osher, 1988). The computations are carried out with the CFL number of 0.6.

Figure 3 shows Schlieren-type images of density at $t = 0.2$ for results calculated with and without multi-scale model. By comparing the results at two resolutions considerably more detailed interface and flow structure are obtained for the multi-scale model. This is not unexpected since the multi-scale model includes the influence of the unresolved-interface interactions which are neglected by the single-scale model due to the loss of unresolved mass, momentum and energy, or due to the wrongly predicted interface interaction based on the ill-defined interface normal direction. To illustrate the potential of the multi-scale method, this case is also simulated with very high-resolution of $\Delta = 1\times10^{-3}$. The Schlieren-type image of density at $t = 0.14$ is shown in Figure 4. It is observed that a very complex wave and interface structures are produced, especially in the roll-up region. These structures show very complex mixing behavior which is totally missing from a previous single-scale simulation at similar resolution (Hu *et al.* 2006).

4. Conclusions

In this work we have proposed a multi-scale method for compressible multi-fluid flow. It consists of a two-scale grid system where the finer grid is used to track the interface by a semi-Lagrangian level set method and the coarser grid to solve the interface interaction and the fluid dynamics. Based on a scale measure, the interface within a computational cell is identified as resolvable or non-resolvable. While the previous conservative sharp-interface method is applied for resolvable interface regions, a mechanical equilibrium interface-interaction model with single pressure and velocity is applied for non-resolvable

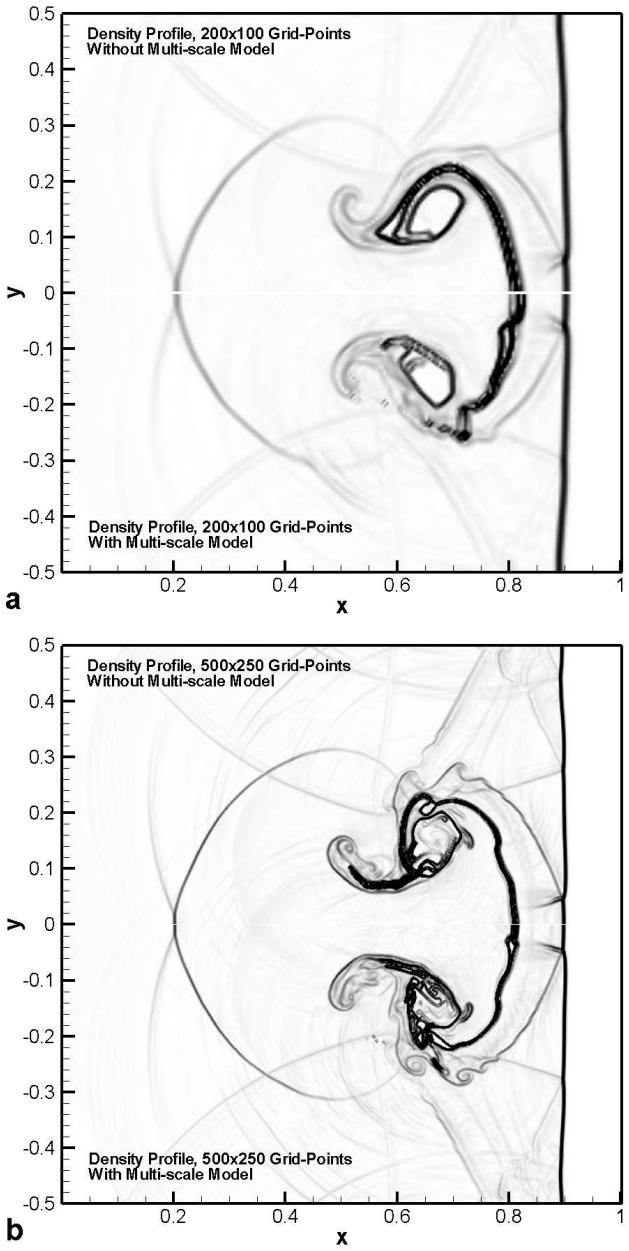

FIGURE 3. Comparison of the results of the shock-bubble interaction problem at time $t = 0.2$: Schlieren-type images (mirrored images from symmetric axes are results with a multi-scale model) of density for (a) $\Delta = 5 \times 10^{-3}$, and (b) $\Delta = 2 \times 10^{-3}$.

interface regions. The coupling between the sharp-interface model and the mechanical equilibrium model is achieved automatically, is fully conservative and reversible and does not require extra modeling. The numerical examples on pure interface transportation and shock-bubble interaction suggest that the multi-scale method produces considerably

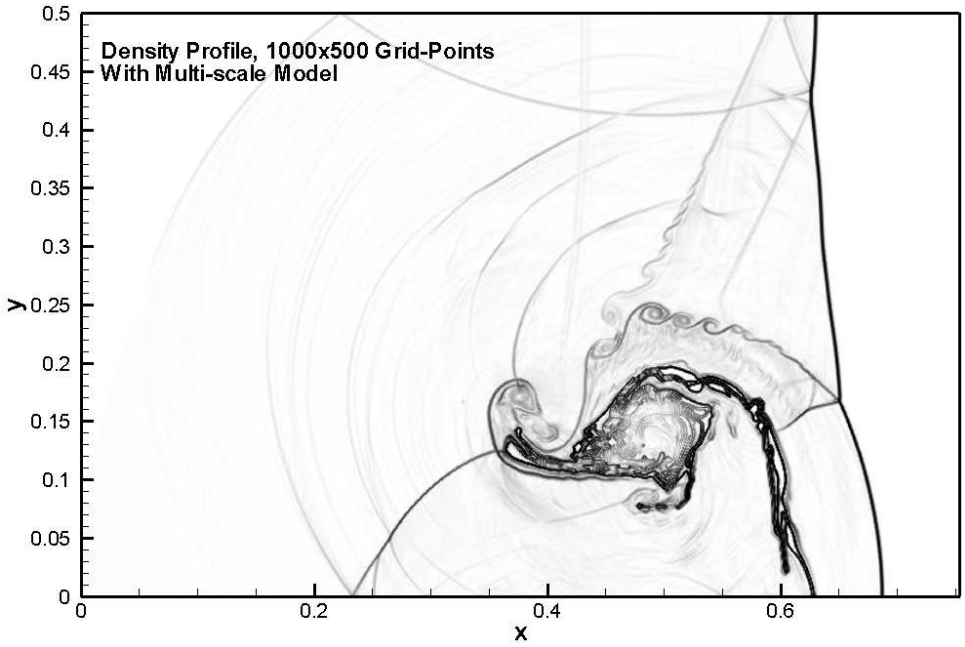

FIGURE 4. The Schlieren-type image of density at $t = 0.14$ for $\Delta = 1 \times 10^{-3}$.

richer interface and flow structures compared to the single scale method at the same grid resolution.

REFERENCES

BELL, J., COLELLA, P., AND GLAZ, H. 1989 A second-order projection method for the incompressible Navier Stokes equations. *J. Comput. Phys.* **85**, 257-283.

FEDKIW, R., ASLAM, T., MERRIMAN, B. AND OSHER, S. 1999 A non-oscillatory Eulerian approch to interfaces in multimaterial flows (the ghost fluid method). *J. Comput. Phys.* **152**, 457-492.

GREENOUGH, J.A., BECKNER, V., PEMBER, R.B., CRUTCHFIELD, W.Y., BELL, J.B. AND COLELLA, P. 1995 An adaptive multifluid interface-capturing method for compressible flow in complex geometries. *AIAA Computational Fluid Dynamics Conference, 12th, and Open Forum, San Diego, CA.*

HARTEN, A. 1996 Multiresolution representation of data: A general framework. *SIAM J. Numer. Analys.* **33**, 1205-1256.

HERMANN, M. 2005 Refined Level Set Grid method for tracking interfaces. *Proceedings of the Summer Program, Center for Turbulence Research, Stanford University.*

HIEBER, S.E. AND KOUMOUTSAKOS, P. 2005 A Lagrangian particle level set method. *J. Comput. Phys.* **210**, 342-367.

HU, X.Y. AND KHOO, B.C. 2004 An interface interaction method for compressible multifluids. *J. Comput. Phys.* **198**, 35-64.

HU, X.Y., KHOO, B.C., ADAMS, N.A. AND HUANG, F.L. 2006 A conservative interface method for compressible flows. *J. Comput. Phys.* **219**, 553-538.

HU, X.Y., ADAMS, N.A., JOHNSEN, E. AND IACCARINO, G. 2008 Modeling full-Mach-

range cavitating flow with sharp interface model. *Proceedings of the Summer Program, Center for Turbulence Research, Stanford University.*

Hu, X.Y., Adams, N.A. and Iacarino, G. 2009 On the HLLC Riemann solver for interface interaction in compressible multi-fluid flow. *J. Comput. Phys.*, **228**, 6572-6589.

Hu, X.Y., Wang, H. and Adams, N.A. 2010 An adaptive central-upwind weighted essentially non-oscillatory scheme. *J. Comput. Phys.*, **229**, 8952-8965.

Jiang, G.S. and Shu, C.W. 1996 Efficient implementation of weighted ENO schemes. *J. Comput. Phys.* **126**, 202-228.

Osher, S. and Sethain, J.A. 1988 Front propagating with curvature dependent speed: algorithm based on Hamilton-Jaccobi formulation. *J. Comput. Phys.* **79**, 12-49.

Pistch, H. 2005 A consistent level set formulation for large-eddy simulation of premixed turbulent combustion. *Combust. Flame* **143**, 587-598.

Shu, C.W. and Osher, S. 1988 Efficient implementation of essentially non-oscillatory shock-capturing schemes. *J. Comput. Phys.* **77**, 439-471.

Strain, J. 1999 Semi-Lagrangian methods for level set equations. *J. Comput. Phys.* **151**, 498-533.